

Mud-Standoff Effect Correction Based on Open-Short Calibration and Resistivity Consistency-Constrained Iterative Inversion for Oil-Based Mud Imagers

Li Fengfeng (email: cj21701@163.com), Feng Zhou, Wu Hongliang,
Zhang Hao, Tian Han, Liu Peng and Yuan Lixin

PetroChina Research Institute of Petroleum Exploration and Development, Beijing 100083, China

January 13, 2026

Abstract

We propose a mud-standoff effect correction method and a set of approximate apparent resistivity inversion methods suitable for oil-based mud micro-resistivity imaging logging. To calibrate the influence of the mud layer on electrode measurement signals, this study integrates the Open-Short calibration(OSC) method with the three-layer impedance model of the oil-based mud resistivity imager. By treating the electrode and the mud layer as an integrated whole and simulating the open/short-circuit states via the finite element method, the independent extraction of the mud layer impedance signal is achieved, and the formation impedance signal is separated from the total impedance. For fast inversion of formation resistivity, standoff thickness (mud layer thickness), and relative permittivity of formation, a resistivity consistency-constrained iterative inversion method is further proposed. In this method, the formation impedance is first converted into resistivity, and then the consistency residual of the resistivity at different frequencies is used as the objective function to invert the approximate apparent resistivity of the formation through an iterative optimization algorithm. The effectiveness of the finite element-simulated OSC method, the objective function construction scheme, and the consistency inversion method is verified through both numerical models and an example of field data.

1 Introduction

With the continuous advancement of oil and gas exploration towards complex domains such as deep formations, high-temperature and high-pressure(HTHP) reservoirs, and shale reservoirs, oil-based mud (OBM) has been widely applied due to its superior lubricity, stability, and adaptability to HTHP conditions. However, the non-conductive nature of OBM makes traditional electrode-type resistivity logging methods inapplicable directly [1], [2]. Compared with water-based mud (WBM) electrical imaging logging, OBM electrical imaging logging based on the capacitive coupling principle employs MHz-level high-frequency signals to drive current through the non-conductive mud and return to the return electrodes. Combined with the multi-frequency measurement mode, it significantly improves the resolution capability for formation resistivity and permittivity [3], [4], [5].

The raw measurement signals of such logging tools are susceptible to interference from mud resistivity, permittivity, and standoff, failing to directly and accurately characterize the true formation information. Currently, techniques such as orthogonal projection, optimization inversion, and machine learning are commonly used to decouple the real and imaginary parts of the raw complex impedance, constructing resistivity-dominated images, permittivity-dominated images, and standoff images, respectively, to effectively separate mud effects from formation properties [6], [7], [8]. Among these methods, the result obtained by orthogonal projection is the stitched formation impedance, whose accuracy largely depends on the calculation precision of the mud impedance phase angle; the vertical/parallel approximation method can achieve rapid calculation of approximate apparent resistivity for formations within a wide dynamic range by calculating apparent resistivity for low-, medium- and high-resistivity formations separately. However, there is still a certain deviation between the equivalent

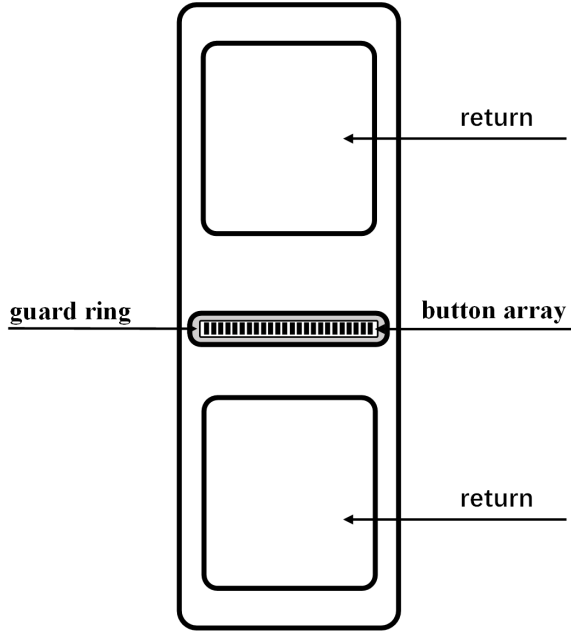


Figure 1: Schematic of fracture model and imaging pads

mud impedance and the actual mud impedance response. Additionally, the final apparent resistivity curve needs to be stitched using segmental thresholds, which introduces inherent uncertainties [9], [10]; although optimization inversion or neural network-driven quantitative inversion methods can achieve higher-precision formation parameter calculation, they have obvious limitations: the former requires pre-construction of large-scale training datasets and exhibits low inversion efficiency, making it difficult to meet the demand for rapid on-site processing; the latter suffers from poor result accuracy and weak controllability of the model prediction process[11], [12].

Open-Short Calibration (OSC) is an impedance calibration technique based on dual extreme state measurements. By acquiring the system's responses under two ideal boundary conditions (complete open circuit and complete short circuit), an error model is constructed to eliminate the deviation introduced by the measurement system itself, thus enabling the accurate extraction of the true impedance of the device under test [13]. In this paper, this technique is extended to correct the interference of the mud layer on electrode measurement signals. We establish a three-layer impedance model ("electrode-mud layer-formation") that integrates the measuring electrode and mud layer as a single system component. Using the finite element method (FEM), we simulate the impedance responses under open- and short-circuit conditions. Based on these simulations, we construct an efficient approximate model through polynomial fitting. Ultimately, we apply the OSC formula to remove mud layer interference and extract the formation impedance.

Theoretically, after converting the complex impedance into resistivity and permittivity, the formation resistivity values at different frequencies should be consistent. Based on this, this paper proposes to use the consistency residual of apparent resistivity at multiple frequencies as the objective function for formation resistivity inversion. The objective function and the corresponding inversion method have been verified through numerical models and field well data. The pad structure of the imaging logging tool adopted in this study is shown in Fig.1, which includes 24 button electrodes, 1 annular focusing electrode, and 2 return electrodes, with two operating frequency modes: F1 (low frequency) and F2 (high frequency).

2 Calculation Methods

2.1 Apparent resistivity and permittivity

The total impedance recorded by the electrode is defined as:

$$Z = \frac{1}{\sigma + i\omega\epsilon\epsilon_0} = \frac{\sigma}{\sigma^2 + \omega^2(\epsilon\epsilon_0)^2} - i\frac{\omega\epsilon\epsilon_0}{\sigma^2 + \omega^2(\epsilon\epsilon_0)^2} \quad (1)$$

where σ is the conductivity (S/m); ϵ is the relative permittivity; ϵ_0 is the permittivity of free space (F/m); ω is the angular frequency (rad/s).

Let the real part of the impedance be $A = \frac{\sigma}{\sigma^2 + \omega^2(\epsilon\epsilon_0)^2}$ and the imaginary part be $B = -\frac{\omega\epsilon\epsilon_0}{\sigma^2 + \omega^2(\epsilon\epsilon_0)^2}$. The ratio of the imaginary part to the real part is expressed as:

$$\frac{B}{A} = -\frac{\omega\epsilon\epsilon_0}{\sigma} \quad (2)$$

Substituting Equation (2) into the expression for the real part of the impedance, we obtain:

$$A = \frac{\sigma}{\sigma^2 + \omega^2 \left(\frac{\sigma B}{\omega A} \right)^2} = \frac{1}{\sigma \left(1 + \frac{B^2}{A^2} \right)} \quad (3)$$

From this, the apparent conductivity is derived as:

$$\sigma_a = \frac{A}{A^2 + B^2} \quad (4)$$

Substituting Equation (4) into Equation (2), the apparent relative permittivity is further obtained:

$$\epsilon_a = -\frac{B}{\omega (A^2 + B^2) \epsilon_0} \quad (5)$$

The total impedance measured by the electrode can be expressed as:

$$Z_{total} = K \frac{U}{I} = A + iB \quad (6)$$

where K is the instrument constant; U is the potential of the button electrode; I is the current of the button electrode.

Combining Equations (4), (5), and (6), the apparent resistivity R_a and apparent relative permittivity ϵ_a are finally expressed as:

$$R_a = \frac{A^2 + B^2}{A} \quad (7)$$

$$\epsilon_a = -\frac{B}{\omega (A^2 + B^2) \epsilon_0} \quad (8)$$

2.2 Open-short calibration for standoff effect correction

The equivalent circuit of electrical imaging logging can be simplified to a series impedance model of the formation and mud layer ($Z_{total} = Z_f + Z_m$). If the accurate mud impedance Z_m can be obtained, the formation impedance Z_f can be derived by subtracting the mud impedance from the total impedance.

1) Equivalent mud impedance

In electrical imaging logging, the electrode is closely attached to the borehole wall, and the current flows vertically from the electrode through the mud into the formation. As a thin layer between the electrode and the formation, the mud can be equivalent to a parallel-plate model, and its impedance is calculated by a series model of parallel-plate capacitance and resistance [7]:

$$Z_m = \frac{d_m}{S} \left(\frac{\sigma_m}{\sigma_m^2 + \omega^2(\epsilon_m\epsilon_0)^2} - i\frac{\omega\epsilon_m\epsilon_0}{\sigma_m^2 + \omega^2(\epsilon_m\epsilon_0)^2} \right) \quad (9)$$

The formation impedance is obtained by subtracting the mud impedance from the total impedance:

$$Z_f = Z_{\text{total}} - K \cdot Z_m = A + iB \quad (10)$$

Substitute the formation impedance Z_f into Equations (7) and (8) to calculate the formation apparent resistivity. It should be noted that there is a certain error between the mud impedance calculated by the equivalent resistance and capacitance and the actual mud impedance, but it can meet the requirements for approximate apparent resistivity calculation in high-resistivity formations [7].

2) Standoff effect correction based on finite element method and OSC method

To accurately separate and calibrate the influence of the mud layer on the measured impedance signal, the Open-Short Calibration (OSC) method is adopted. The core idea of this method is: under the same geometric structure, measure the impedance responses under two extreme boundary conditions (open circuit and short circuit) respectively to construct an equivalent circuit model, and then separate the impedance contribution of the mud from the measured total impedance.

As shown in Fig.2, the calibration model consists of three layers: the outermost layer is an ideal conductor (short-circuit state) or air (open-circuit state), the middle layer is the mud to be calibrated, and the inner layer is the measuring pad. Let the total measured impedance be Z_{total} , the mud impedance be Z_m , the pad impedance be Z_b , and the external medium impedance be Z_{ext} .

In the short-circuit state, the external medium is an ideal conductor with approaches zero, and the total impedance of the measurement system is approximately:

$$Z_{\text{short}} = Z_m + Z_b \quad (11)$$

In the open-circuit state, the external medium is air with approaches infinity, and the total impedance of the measurement system is approximately:

$$Z_{\text{open}} = Z_{\text{air}} + Z_m + Z_b \quad (12)$$

The open-circuit state provides the maximum external impedance reference. Taking the open-circuit state as the "zero-signal" reference, the effective admittance change is defined as:

$$Y_{\text{eff}} = \frac{1}{Z_{\text{total}} - Z_{\text{short}}} - \frac{1}{Z_{\text{open}} - Z_{\text{short}}} \quad (13)$$

where $Z_{\text{total}} - Z_{\text{short}} = Z_b + Z_m$, $Z_{\text{open}} - Z_{\text{short}} = Z_{\text{air}}$

The external medium impedance can be obtained through short-circuit calibration. However, when the formation resistivity is relatively high, retaining the second term for differential calibration can further improve the calculation accuracy. At this time, the formation impedance after open-short calibration is expressed as:

$$Z_f = Z_C = \left[\frac{1}{Z_{\text{total}} - Z_{\text{short}}} - \frac{1}{Z_{\text{open}} - Z_{\text{short}}} \right]^{-1} \quad (14)$$

The finite element method is used to simulate the measured impedance under open-circuit and short-circuit states. Fig.3 shows the comparison results between the measured impedance amplitude, phase angle calculated in the short-circuit state and the equivalent mud impedance: the phase angles are consistent, but the amplitudes differ significantly. A fourth-order polynomial (Eq.15) is used for piecewise fitting of the equivalent mud impedance amplitude and the finite element-calculated mud impedance amplitude. The fitting results, as shown in Fig.4, have a relative error of less than 0.5% between the fitted values and the true values.

Similarly, a fourth-order polynomial is used to fit the measured impedance in the open-circuit state. The relative errors of the fitted impedance amplitude and phase are shown in Fig.5, with the maximum relative error not exceeding 2.5%. Subsequently, the efficient calculation of impedance under open-circuit and short-circuit states will be achieved using the fitting results and the equivalent mud impedance phase.

$$\begin{aligned} A_{\text{True}} = & c_0 + \\ & c_1 A + c_2 A^2 + c_3 A^3 + c_4 A^4 + \\ & c_5 d_m + c_6 d_m^2 + c_7 d_m^3 + c_8 d_m^4 + \\ & c_9 d_m A + c_{10} d_m A^2 + c_{11} d_m A^3 + \\ & c_{12} d_m^2 A + c_{13} d_m^2 A^2 + c_{14} d_m^3 A \end{aligned} \quad (15)$$

2.3 Objective function of consistency inversion

Under the same formation resistivity condition, the impedance measured by the imaging tool at different frequencies shows significant frequency-dependent differences due to the influence of the borehole environment, dielectric constant, and other factors. Considering that the relative permittivity of the formation has frequency dispersion characteristics while the resistivity is non-dispersive, there should be a unique solution when inverting formation resistivity from multi-frequency impedance data. We construct an optimization objective function constrained by the consistency of apparent resistivity, and realize the iterative inversion of formation apparent resistivity by minimizing the residual of apparent resistivity between different frequencies.

The objective function is constructed as the residual of apparent resistivity at each frequency:

$$F = \left\| \frac{R_{a,1} - R_{a,2}}{R_{a,2}} \right\| \quad (16)$$

In the inversion process, 5 parameters need to be iteratively optimized: the mud resistivity at two frequencies, the mud relative permittivity at two frequencies, and the mud thickness. The calculation process is as follows:

- 1) Set the initial values and search ranges of mud resistivity, permittivity, and standoff. 2) Calculate the mud impedance and the approximate apparent resistivity of the formation at different frequencies based on the initial values;
- 3) Substitute the approximate apparent resistivity into Eq. 13 to compute the objective function value;
- 4) Iterate via the optimization algorithm until the objective function value meets the allowable precision.

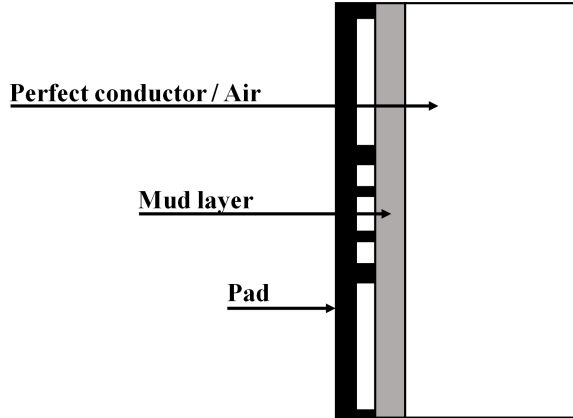


Figure 2: The calculation model of OSC

3 Methods validation

3.1 Validation of the OSC method for standoff effect correction

To validate the correction effect of the OSC method on the standoff effect, the vertical coupling apparent resistivity, parallel coupling apparent resistivity [7], and the apparent resistivity calculated by the OSC method were compared and analyzed under the excitation frequencies of 1 MHz and 30 MHz (Figs.6-9).

Fig.6 shows the apparent resistivity results calculated by the three methods under the conditions of mud resistivity $10000 \Omega \cdot m$, mud relative permittivity 8, standoff 1 mm, and formation relative permittivity 20. It can be seen that the apparent resistivity calibrated by OSC has good continuity, which is basically consistent with the spliced vertical/parallel coupling apparent resistivity.

Fig.7 and Fig.8 compare the apparent resistivity calculation results under different formation permittivities and different standoffs, respectively. The analysis shows that when the formation relative

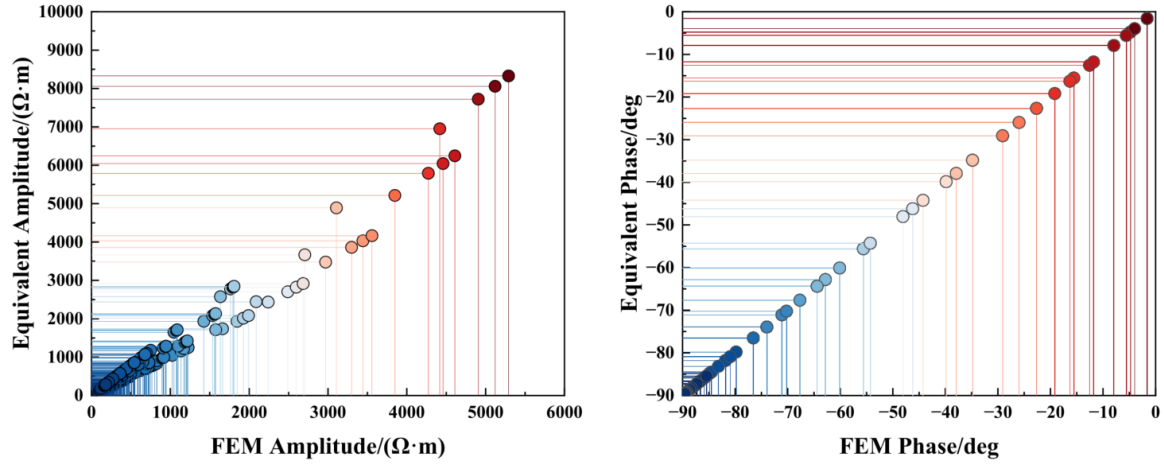


Figure 3: Comparison of mud impedance amplitude and phase

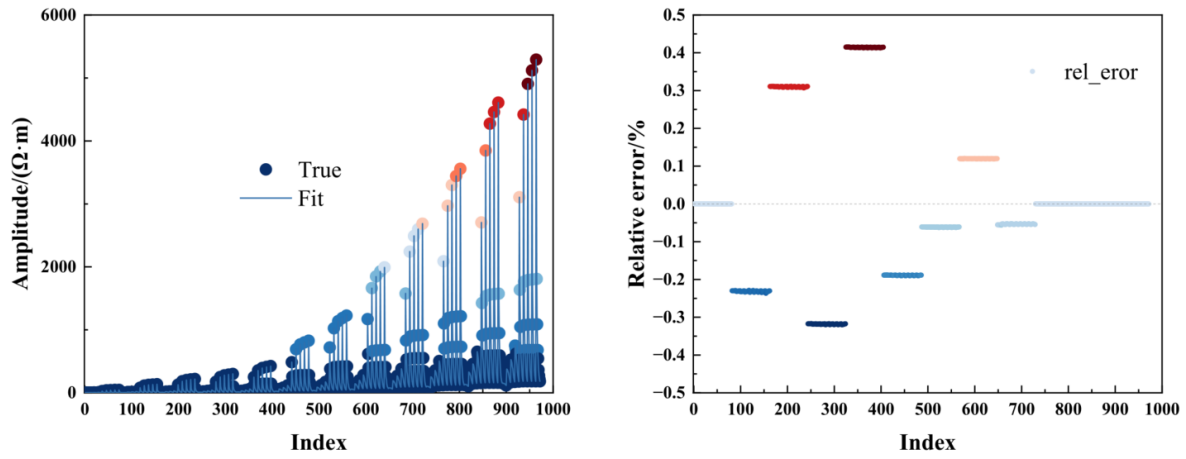


Figure 4: The fitting results of mud impedance amplitude

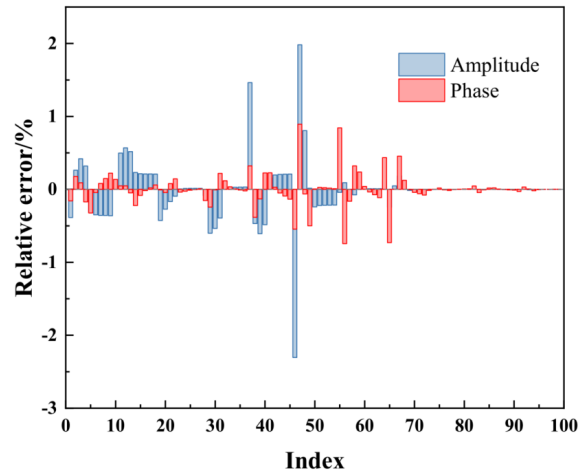


Figure 5: The relative error of impedance and phase in the open state

permittivity is less than 100, the apparent resistivity calculated by the OSC method changes approximately linearly; when it is greater than 100, although the growth rate of apparent resistivity in high-resistivity formations slows down, the apparent resistivity can still be effectively calculated. In contrast, the calculable range of the vertical/parallel coupling method shrinks significantly with the increase of formation permittivity; the standoff has little effect on the OSC method, while the calculable range of the vertical/parallel coupling method decreases with the increase of standoff.

In general, the OSC method has a better correction effect on the impedance contribution of the mud layer than the vertical/parallel coupling method, and has a wider range of correctable formation resistivity. Moreover, a complete apparent resistivity curve can be obtained without splicing, which significantly reduces the uncertainty of the results.

Fig.9 compares the apparent resistivity results of open-circuit-short-circuit combined calibration and short-circuit-only calibration. It can be seen that there is a certain difference between the two only in ultra-high resistivity formations with large standoff; in most cases, a high-precision apparent resistivity curve can be obtained by using only short-circuit calibration.

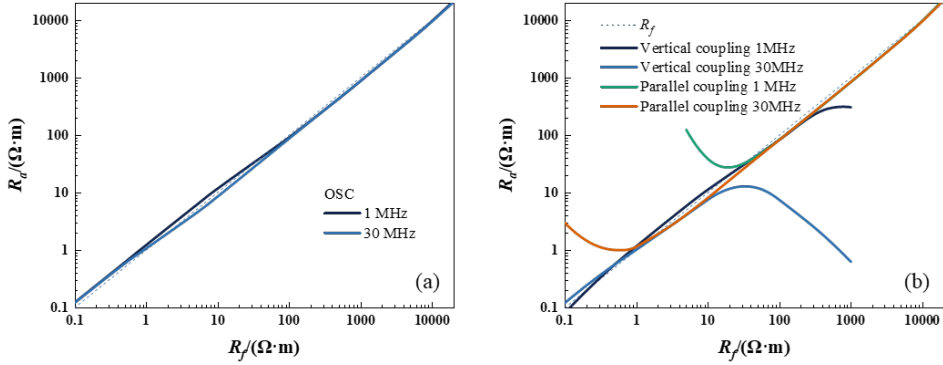


Figure 6: OSC corrected and vertical/parallel coupling results ($R_m = 10000 \Omega \cdot \text{m}$, $\varepsilon_m = 8$, $stdf = 1$ mm, $\varepsilon_f = 20$)

3.2 Validation of the objective function

The mud resistivity was set to $10000 \Omega \cdot \text{m}$, the mud relative permittivity was set to 6, and the standoff was set to 1 mm. Fig.10 presents the apparent resistivity calculation results under different deviated mud parameters, where Fig.10(a) shows the case of deviated standoff from the true value, and Fig.10(b) shows that of deviated mud resistivity. As can be seen from the figure: when the mud parameters are properly selected, the apparent resistivities at the two frequencies exhibit the best consistency, and their ratio is closest to 1; when the mud parameters are improperly selected, the apparent resistivities become discrete, with significant differences between the results at the two frequencies; the mud resistivity has a relatively small impact on the apparent resistivity calculation results. Even if its value is inaccurate, the calculated apparent resistivities are still very close to the true values within a certain range of formation resistivity.

As shown in Fig. 11, the distribution of objective function values under different mud relative permittivities and standoffs is presented. The minimum objective function value occurs when the mud relative permittivity $\varepsilon_m = 6$ and the standoff is 1, which further validates the feasibility of the resistivity-consistency-based iterative inversion method.

The Gauss-Newton algorithm was used to invert the formation model containing three fractures filled with different materials. The formation model parameters were referenced from Ref.[8] (Fig.12): standoff was 1.54 mm; at frequency 1, the mud resistivity was $8400 \Omega \cdot \text{m}$ and the relative permittivity was 12; at frequency 2, the mud resistivity was $339 \Omega \cdot \text{m}$ and the relative permittivity was 10; the formation resistivity was $30 \Omega \cdot \text{m}$, and the relative permittivities at the two frequencies were 38 and 19, respectively; the fracture spacing was set to 20 mm, the fracture apertures were all 6.35 mm, and the fracture resistivities increased sequentially. The inversion results are shown in Fig.13, including the curves of apparent resistivity, mud thickness and relative permittivity at high frequency. From the inversion results, it can be concluded that: for the formation model with frequency dispersion characteristics, the consistency iterative inversion method still maintains good stability, and the inverted

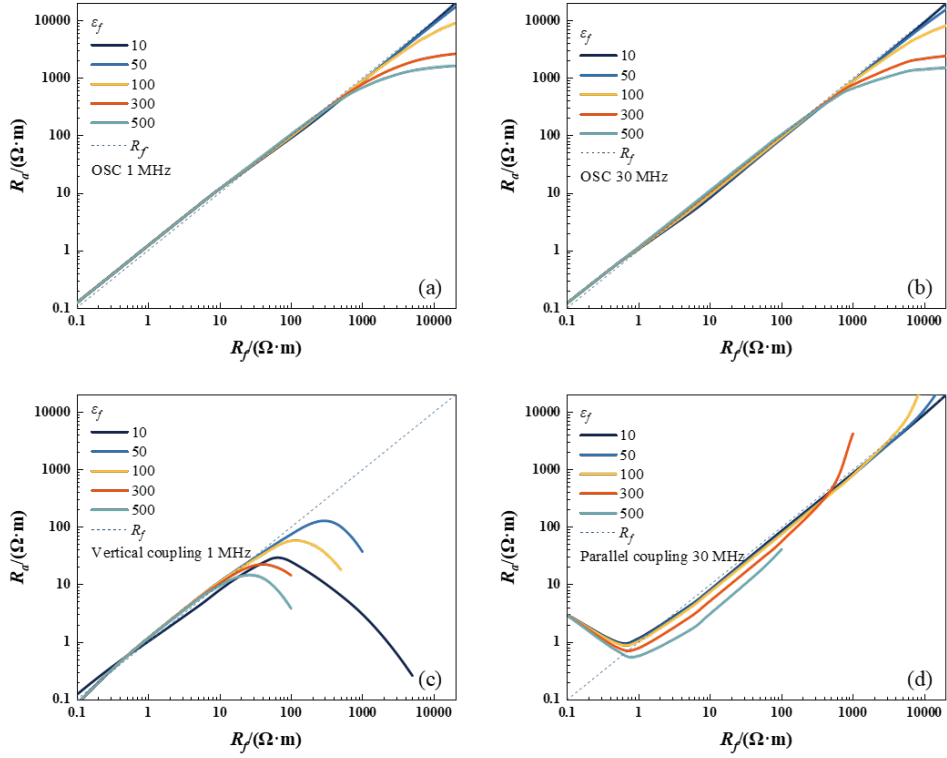


Figure 7: Apparent resistivity results under different formation permittivities ($R_m = 10000 \Omega \cdot \text{m}$, $\varepsilon_m = 8$, $stdf = 1 \text{ mm}$, $\varepsilon_f = 20$). (a) OSC corrected at 1 MHz. (b) OSC corrected at 30 MHz. (c) Vertical Approximation at 1 MHz. (d) Parallel Approximation at 30 MHz

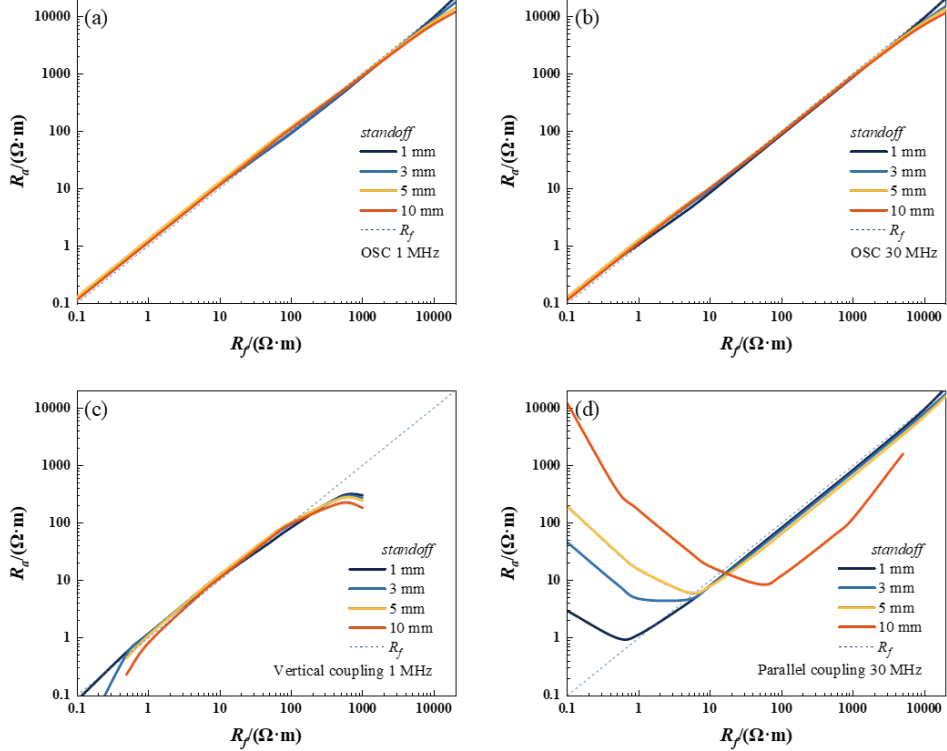


Figure 8: Apparent resistivity results under different standoffs ($R_m = 10000 \Omega \cdot \text{m}$, $\varepsilon_m = 8$, $\varepsilon_f = 20$). (a) OSC corrected at 1 MHz. (b) OSC corrected at 30 MHz. (c) Vertical coupling at 1 MHz. (d) Parallel coupling at 30 MHz

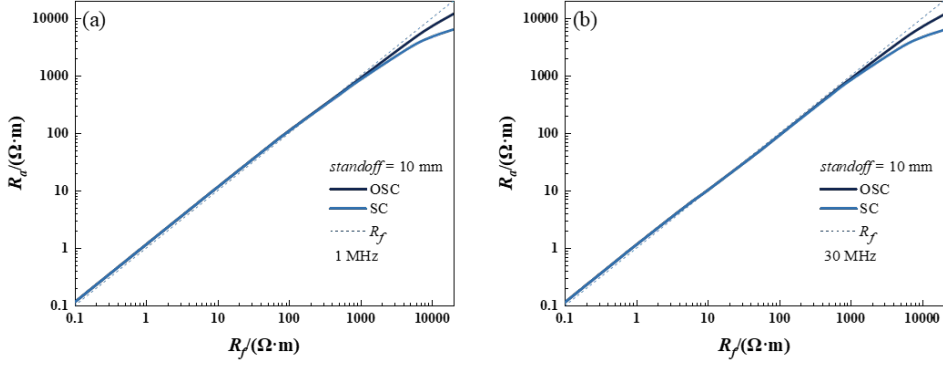


Figure 9: Comparison of open-short calibration and short calibration results ($R_m = 10000 \Omega \cdot \text{m}$, $\epsilon_m = 8$, $stdf = 10 \text{ mm}$). (a) Corrected Result at 1 MHz. (b) Corrected Result at 30 MHz.

parameters can clearly reflect the changes in formation physical properties; the apparent resistivity curve is more sensitive to low-resistivity fractures; in high-resistivity fractures, the response of the standoff curve is more obvious, especially when the fractures are filled with mud; the variation trend of the relative permittivity curve at frequency 2 is opposite to that of the resistivity curve.

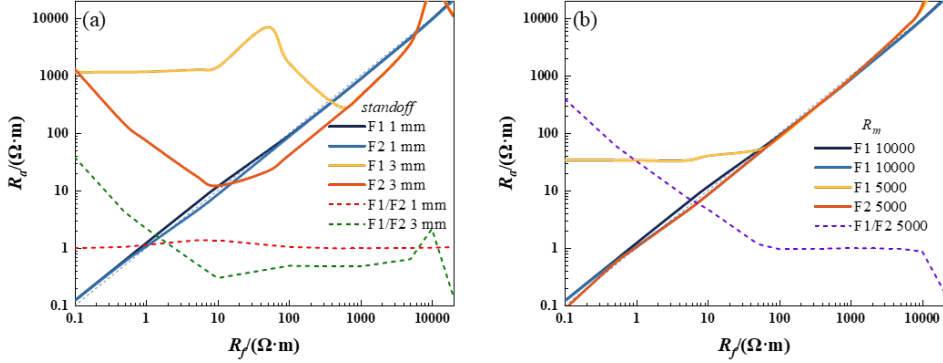


Figure 10: Validation of the resistivity consistency

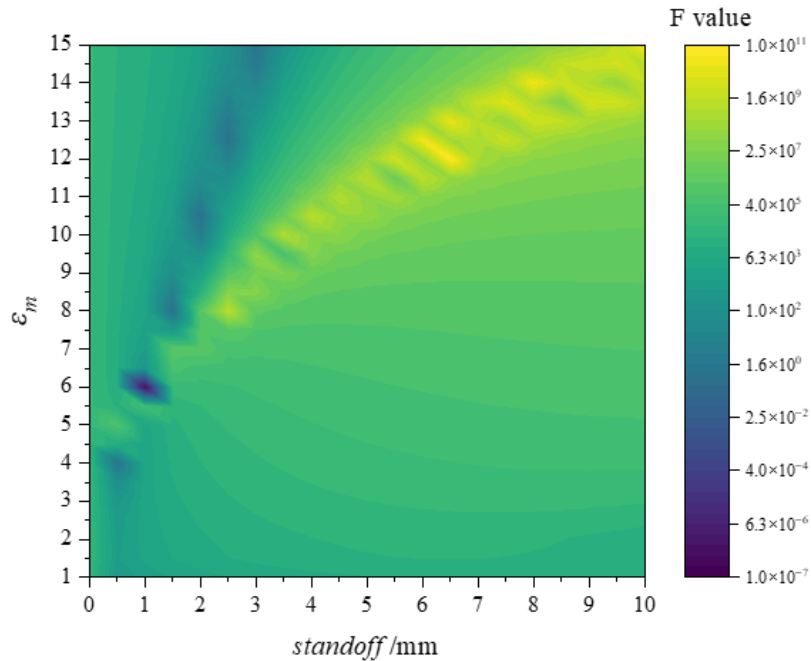


Figure 11: The distribution of objective function values

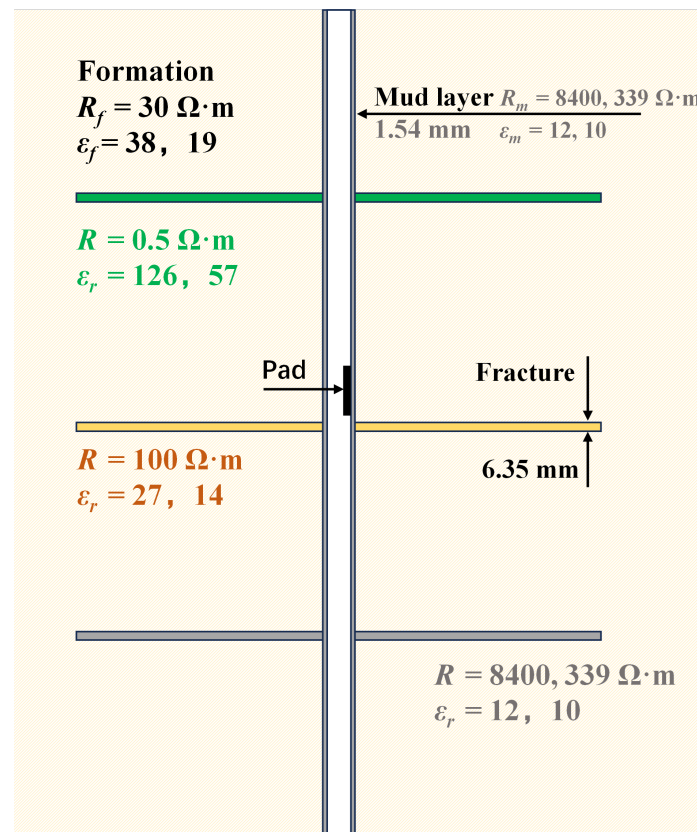


Figure 12: The fractured formation models

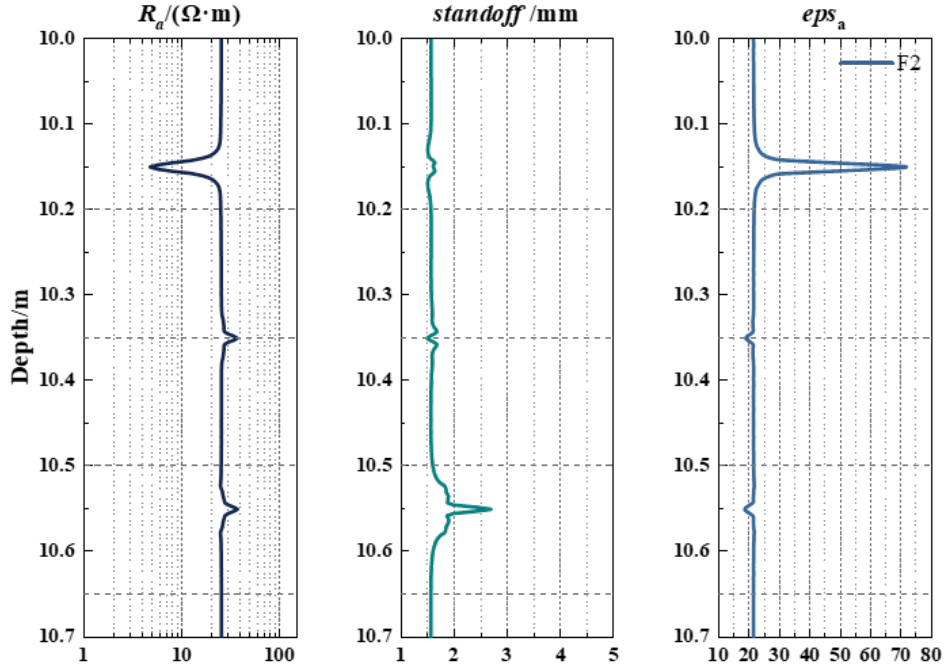


Figure 13: Resistivity consistency inversion results for fractured formations

4 Conclusions

We introduce the open-short calibration method into the measurement signal processing of the oil-based mud resistivity imagers, and propose a new mud impedance calculation method. The measurement system is modeled as a three-layer model including the impedances of the electrode, mud layer, and external medium. The finite element method is used to simulate the impedance responses under open-circuit and short-circuit states, and the calibration formula is applied to eliminate the signals from the system and mud, thus effectively separating the formation signal. Validations on multiple models show that this method is superior to the vertical/parallel coupling method. It can realize full-range resistivity calculation from low-resistivity to high-resistivity formations and avoid the uncertainty caused by resistivity threshold splicing.

Taking the multi-frequency resistivity consistency residual as the objective function, we propose an approximate apparent resistivity consistency iterative inversion method. Only a small number of datasets need to be pre-constructed for this method, which can complete the optimal solution of 5 parameters (mud layer parameters) through 4 measured values, realizing the inversion of formation apparent resistivity, permittivity, interval and other parameters. The calculation efficiency is 2-3 times higher than that of quantitative inversion. The analysis and verification of the defined objective function show that when the mud layer parameters are reasonably selected, the objective function attains the minimum value, indicating that the resistivity consistency residual can be used to invert the formation resistivity. The theoretical verification on the fractured formation model and the application test on the case well show that the consistency inversion can effectively calculate the formation characteristics. Although it is an approximate processing method, its inversion results are highly consistent with the quantitative inversion results.

References

[1] P. Schlicht, T. Zhang, M. G. Lüling, B. R. Graham, A. Cournot, and R. Sadownyk, “Identifying fracture-filling material in oil-based mud with dielectric borehole imaging,” in *SPWLA Annual Logging Symposium*, p. D083S005R001, SPWLA, 2020.

- [2] V. Hilton, A. Sapru, and M. Pavlovic, “Detailed reservoir characterization utilizing oil-based micro-resistivity image logs,” in *SPWLA Annual Logging Symposium*, pp. SPWLA–2003, SPWLA, 2003.
- [3] Y. Wu, B. Lu, W. Zhang, Y. Jiang, B. Wang, and Z. Huang, “A new logging-while-drilling method for resistivity measurement in oil-based mud,” *Sensors*, vol. 20, no. 4, p. 1075, 2020.
- [4] G. Itsikovich, B. Corley, S. Forgang, and F. Le, “An improved resistivity imager for oil-based mud: basic physics and applications,” *SPWLA 55th Annual Logging Symposium, Abu Dhabi, United Arab Emirates: Society of Petrophysicists and Well Log Analysts*, 2014.
- [5] J. Gao, L. Jiang, Y. Liu, and Y. Chen, “Review and analysis on the development and applications of electrical imaging logging in oil-based mud,” *Journal of Applied Geophysics*, vol. 171, p. 103872, 2019.
- [6] Y.-H. Chen, D. Omeragic, T. Habashy, R. Bloemenkamp, T. Zhang, P. Cheung, and R. Laronga, “Inversion-based workflow for quantitative interpretation of the new-generation oil-based-mud resistivity imager,” *Petrophysics*, vol. 55, no. 06, pp. 554–571, 2014.
- [7] J. Gao, J. Sun, Y. Jiang, L. Cui, P. Zhang, and J. Wu, “A novel quantitative imaging method for oil-based mud: the full-range formation resistivity,” *Journal of Petroleum Science and Engineering*, vol. 162, pp. 844–851, 2018.
- [8] Y.-H. Chen, T. Zhang, R. Bloemenkamp, and L. Liang, “Fracture imaging and response characterization of the high-definition oil-based mud borehole imagers through modeling and inversion,” *Petrophysics-The SPWLA Journal of Formation Evaluation and Reservoir Description*, vol. 64, no. 04, pp. 544–554, 2023.
- [9] J. Sun, J. Gao, Y. Jiang, and L. Cui, “Resistivity and relative permittivity imaging for oil-based mud: a method and numerical simulation,” *Journal of Petroleum Science and Engineering*, vol. 147, pp. 24–33, 2016.
- [10] B. Guner, A. E. Fouda, W.-B. Ewe, D. Torres, and P. Barrett, “Quantitative demonstration of a high-fidelity oil-based mud resistivity imager using a controlled experiment,” *Petrophysics*, vol. 62, no. 04, pp. 407–421, 2021.
- [11] Z. Bayraktar, D. Omeragic, and Y.-H. Chen, “Quantitative interpretation of oil-base mud microresistivity imager via artificial neural networks,” in *SPWLA Annual Logging Symposium*, p. D043S005R003, SPWLA, 2019.
- [12] J.-s. Gao, J.-p. Zhao, and X.-f. Li, “Optimization of microresistivity imaging logging in oil-based drilling fluid based on ga-bp neural network,” in *International Field Exploration and Development Conference*, pp. 1795–1804, Springer, 2019.
- [13] Y. Li and L. Zhu, “A short–open calibration method for accurate de-embedding of 3-d nonplanar microstrip line structures in finite-element method,” *IEEE Transactions on Microwave Theory and Techniques*, vol. 66, no. 3, pp. 1172–1180, 2017.